HHS Public Access

Author manuscript

J Vis Exp. Author manuscript; available in PMC 2024 May 26.

Ex Vivo OCT-Based Multimodal Imaging of Human Donor Eyes for Research in Age-Related Macular Degeneration

Jeffrey D. Messinger[1], **Max Brinkmann**[2], **James A. Kimble**[1], **Andreas Berlin**[1], **K. Bailey Freund**[3,4], **Gregory H. Grossman**[5], **Thomas Ach**[*,6], **Christine A. Curcio**[*,1]

[1]Department of Ophthalmology and Visual Sciences, University of Alabama at Birmingham Heersink School of Medicine, Birmingham AL USA

[2]Department of Ophthalmology, University Hospital of Zurich, Switzerland

[3]Vitreous Retina Macula Consultants of New York NY USA

[4]Department of Ophthalmology, New York University Grossman School of Medicine, New York NY, USA

[5]Advancing Sight Network, Birmingham AL USA

[6]University Hospital Bonn, Department of Ophthalmology, Bonn Germany

Abstract

A progression sequence for age-related macular degeneration (AMD) learned from optical coherence tomography (OCT) based multimodal (MMI) clinical imaging could add prognostic value to laboratory findings. E*x vivo* OCT and MMI were applied to human donor eyes prior to retinal tissue sectioning. Eyes were recovered from non-diabetic white donors ≥80 years old, with death to preservation time (DtoP) ≤6 h. Globes were recovered on-site, scored with an 18-mm trephine to facilitate cornea removal, and immersed in buffered 4% paraformaldehyde. Color fundus images were acquired after anterior segment removal with a dissecting scope and an SLR camera using trans-, epi-, and flash illumination at three magnifications. Globes were placed in a buffer within a custom-designed chamber with a 60-diopter lens. They were imaged with spectral domain OCT (30° macula cube, 30 μm spacing, averaging = 25), near-infrared reflectance, 488 nm autofluorescence, and 787 autofluorescence. AMD eyes showed a change in retinal pigment epithelium (RPE) with drusen or subretinal drusenoid deposits (SDD), with or without neovascularization, and without evidence of other causes. Between 06/16–09/17, 94 right eyes and 90 left eyes were recovered (DtoP, 3.9 ± 1.0 h). Of 184 eyes, 40.2% had AMD: early intermediate (22.8%), atrophic (7.6%), neovascular (9.8%), and 39.7% had unremarkable maculas. Drusen, SDD, hyperreflective foci, atrophy, and fibrovascular scars were identified in OCT. Artifacts included tissue opacification, detachments (bacillary, retinal, RPE, choroidal),

Corresponding author: Christine A. Curcio (christinecurcio@uabmc.edu).
*co-senior authors

A complete version of this article that includes the video component is available at http://dx.doi.org/10.3791/65240.

DISCLOSURES:
CAC receives research support from Heidelberg Engineering and consults for Apellis, Astellas, Boehringer Ingelheim, Character Bioscience, and Osanni. TA receives research support from Novartis and consults for Roche, Novartis, Bayer, Nidek, Apellis. KBF is a consultant to Genentech, Zeiss, Heidelberg Engineering, Allergan, Bayer, and Novartis.

foveal cystic change, undulating RPE, and mechanical damage. To guide cryo-sectioning, OCT volumes are used to find fovea and optic nerve head landmarks and specific pathologies. *Ex vivo* volumes are registered with *in vivo* volumes by selecting the reference function for eye tracking. *Ex vivo* visibility of pathology seen *in vivo* depends on preservation quality. Within 16 months, 75 rapid DtoP donor eyes at all stages of AMD were recovered and staged using clinical MMI methods.

SUMMARY:

Laboratory assays can leverage prognostic value from longitudinal optical coherence tomography (OCT) based multimodal imaging of age-related macular degeneration (AMD). Human donor eyes with and without AMD are imaged using OCT, color, near-infrared reflectance scanning laser ophthalmoscopy, and autofluorescence at two excitation wavelengths prior to tissue sectioning.

Keywords

eye banking; biobanking; optical coherence tomography; multimodal imaging; age-related macular degeneration

INTRODUCTION:

Fifteen years of managing neovascular age-related macular degeneration (AMD) with anti-VEGF therapy under the guidance of optical coherence tomography (OCT) has offered new insights into the progression sequence and microarchitecture of this prevalent cause of vision loss. A key recognition is that AMD is a three-dimensional disease involving the neurosensory retina, retinal pigment epithelium (RPE), and choroid. Thanks to OCT imaging of trial patients and fellow eyes of treated clinic patients, features of pathology beyond those seen by color fundus photography, a clinical standard for decades, are now recognized. These include intraretinal neovascularization (type 3 macular neovascularization[1], formerly angiomatous proliferation), subretinal drusenoid deposits (SDD, also called reticular pseudodrusen),[2] multiple pathways of RPE fate[3,4], and intensely gliotic Müller cells in atrophy.[5,6]

Model systems lacking maculas (cells and animals) re-create some slices of this complex disease[7–9]. Further success in ameliorating the burden of AMD can come from the discovery and exploration of primary pathology in human eyes, respecting the unique cellular composition of the macula, followed by translation to model systems. This report portrays a 3-decade collaboration between an academic research laboratory and an eye bank. The goals of the tissue characterization methods described herein are two-fold: 1) to inform evolving diagnostic technology by demonstrating with microscopy the basis of fundus appearance and imaging signal sources, and 2) to classify AMD specimens for targeted (immunohistochemistry) and untargeted molecular discovery techniques (imaging mass spectrometry, IMS, and spatial transcriptomics) that preserve the cone-only fovea and rod-rich para- and perifovea. Such studies could accelerate translation to clinical OCT, where a progression sequence and longitudinal follow-up are possible through eye-tracking. Designed to monitor treatment effects, this technology registers scans from one clinic visit to

the next using retinal vessels. Linking eye-tracked OCT to laboratory results obtained with destructive techniques could provide a new level of prognostic value to molecular findings.

In 1993 the research laboratory captured color photographs of postmortem fundus on film[10]. This effort was inspired by superb photomicroscopy and histology of the human peripheral retina by Foos and associates[11–13] and extensive AMD clinicopathologic correlations by Sarks, Sarks, and Killingsworth[14,15]. Starting in 2009, *ex vivo* multimodal imaging (MMI) anchored on spectral domain OCT was adopted. This transition was inspired by similar efforts of others[16,17] and especially by the realization that so much ultrastructure described by the Sarks was available in three dimensions, over time, in the clinic[18,19]. The goal was to acquire eyes with attached maculas, in a reasonable time frame, for well-powered studies of cellular-level phenotypes in retina, RPE, and choroid. The intent was to move beyond “per eye” statistics to “per lesion type,” a standard influenced by “vulnerable plaque” concepts from cardiovascular disease[20,21]

The protocol in this report reflects experience with nearly 400 pairs of donor eyes, accessioned in several streams. In 2011–2014, the Project MACULA website of AMD histopathology was created, with layer thicknesses and annotations from 142 archived specimens. These eyes were preserved from 1996–2012 in a glutaraldehyde-paraformaldehyde fixative for high-resolution epoxy-resin histology and electron microscopy. All fundi had been photographed in color when received and were re-imaged by OCT just prior to histology. An eye holder originally designed for optic nerve studies[22] was used to accommodate an 8-mm-diameter full-thickness tissue punch centered on the fovea. OCT B-scans through the foveal center and a site 2 mm superior, corresponding to histology at the same levels, were uploaded to the website, plus a color fundus photograph. The choice of OCT planes was dictated by the prominence of AMD pathology under the fovea[23] and the prominence of SDD in rod-rich areas superior to the fovea[24,25].

Starting in 2013, eyes imaged with OCT-anchored MMI during life were available for direct clinicopathologic correlations. Most (7 of 10 donors) involved patients at a retina referral practice (author KBF), which offered an advanced directive registry for patients interested in donating eyes after death for research purposes. Eyes were recovered and preserved by the local eye bank, transferred to the laboratory, and prepared the same way as the Project MACULA eyes. Pre-mortem clinical OCT volumes were seamlessly read in the laboratory, thus aligning pathology features seen during life with features seen under the microscope[26].

Starting in 2014, prospective eye collection began by screening for AMD in donor eyes without clinical history but preserved during a defined time limit (6 hours). For this purpose, the eye holder was modified to accommodate a whole globe. This reduced the chance of detachment around the cut edges of the previously used 8 mm punch. Eyes were preserved in 4% buffered paraformaldehyde for immunohistochemistry and transferred to 1% the next day for long-term storage. In 2016–2017 (pre-pandemic), 184 eyes of 90 donors were recovered. The statistics and images in this report are generated from this series. During the pandemic era (2020 lockdowns and aftermath), prospective collections for transcriptomics and IMS collaborations continued at a reduced pace, using essentially the 2014 methods.

Other methods for donor eye assessment are available. The Minnesota Grading System (MGS)[27,28] is based on the AREDS clinical system for color fundus photography[29]. Limitations include the combining of atrophic and neovascular AMD into one stage of "late AMD". Further, the MGS entails the removal of the neurosensory retina before photo-documentation of the RPE-choroid. This step dislodges SDD to varying degrees[30,31] and removes the spatial correspondence of the outer retina and its support system. Thus, efforts to link metabolic demand and signaling from the retina to pathology in RPE-choroid may be impeded. The Utah System implemented MMI using *ex vivo* color photography and OCT to categorize eyes destined for dissection into regions for RNA and protein extractions[32]. Although preferable to whole eye-cup extractions, the 3-mm-diameter area at the highest risk for AMD progression[33,34] represents only 25% of a 6-mm diameter fovea-centered punch. Thus, techniques that can localize findings in reference to the fovea, such as serial sectioning for immunohistochemistry, are advantageous.

PROTOCOL:

The institutional review board at the University of Alabama at Birmingham approved the laboratory studies, which adhere to Good Laboratory Practices and Biosafety Level 2/2+. All US eye banks conform to the 2006 Uniform Anatomical Gifts Act and US Food and Drug Administration. Most US eye banks, including Advancing Sight Network, conform to the regulations of the Eye Bank Association of America.

Table of Materials lists supplies and equipment. Supplementary Material 1 provides an overview of dissection, color fundus photography, and OCT-based MMI. Supplementary Material 2 provides details of OCT-based MMI.

1. Criteria for tissue collection

1.1. To maximize the yield of AMD eyes in a screen of undocumented donors, set the following criteria for acceptable donors: age ≥ 80 years, white, non-diabetic, and ≤6 h death-to-preservation (DtoP).

Note: DtoP is defined as the time between death and when the eye is placed in a provided preservative, either in the hospital or the laboratory.

2. Preservation medium and other preparation (laboratory)

2.1. Make 4% phosphate-buffered paraformaldehyde from 20% stock (purchased). Prepare 1 liter by 200 mL of 20% paraformaldehyde (dilution factor of 5) to 800 mL of 0.1 M Sorenson's phosphate buffer. Test and adjust for pH = 7.2 if necessary. Store at 4 ˚C.

2.2. Dispense 30 mL of 4% phosphate-buffered paraformaldehyde into 40 mL jars.

2.3. Stock labeled 40 mL containers of preservative at the eye bank so that tissue can be recovered at any time or day.

2.4. For storage of preserved eyes, make 1% paraformaldehyde from the 4% solution. Prepare 1 L by adding 250 mL of 4% paraformaldehyde (dilution

factor of 4) to 750 mL of 0.1 M Sorenson's phosphate buffer. Test and adjust for pH if necessary. Store at 4 ˚C.

2.4.1 Prepare a 1 L of 0.1 M solution from the 0.2 M solution of Sorenson's phosphate buffer, pH 7.2 by adding 500 ml of distilled water and 500 ml of Sorenson's buffer.

2.4.2 Adjust pH drop by drop by using 1 N hydrochloric acid or 1 N of sodium hydroxide. Store at 4 ˚C.

2.5. Create a holder to stabilize eyes during dissection. Fill a Petri dish with dental wax heated until liquid. When it is slightly cool, make a hemispheric impression in it with a large ball bearing, then freeze the dish to facilitate the removal of the ball bearing.

3. Eye bank methods

3.1. To ensure rapid recovery of research tissues, recover all tissues rapidly, including those intended for transplantation.

2.2. Receive death referrals, as required by law, within 1 h of death, and track each donor with a referral sequence number that follows the tissue.

3.3. To find cases with potential clinical documentation, ask AMD- and eye disease-specific questions in the research Donor Risk Assessment Interview.

3.4. To minimize travel time, recover whole globes (as distinct from only corneas for transplantation) within a compact area, i.e., city and adjacent suburban county.

3.5. Bring two jars of preservative (buffered 4% paraformaldehyde) to the decedent's hospital room for tissue recovery (as opposed to waiting for the body to be moved to a morgue).

3.6. Before and during recovery, communicate with investigators to confirm delivery and timing.

3.7. Recover globes on-site in the hospital, open them by consistent handling methods, and immerse the opened eye in preservative (Figure 1).

3.7.1. Hold the excised donor eye in place by a sheath of gauze stabilized by a hemostat.

3.7.2. To facilitate removal of the cornea with a 2-mm-wide rim of sclera, use an 18 mm diameter trephine to score the globe.

3.7.3. To free the cornea with an accompanying rim of sclera, cut along the scored circle using spring-loaded scissors with curved tips, while stabilizing the globe with the hemostat-clipped gauze.

3.7.4. Lift the cornea off the sclera, exposing the iris and ciliary body.

3.7.5. To facilitate preservative penetration into the vitreous chamber, make a 2-mm-long slit in the iris, perpendicular to the pupillary

margin. Place eyes into specimen jars with 30 mL of preservative at 4 °C and transfer to the laboratory on wet ice.

3.8. Transmit de-identified donor information electronically from the eye bank to the research laboratory database. Note: The database maintains the referral number, an eye bank tissue number, and a laboratory ID number for tracking, plus other relevant information.

4. Tissue preparation for *ex vivo* color fundus photography

4.1. Use two stereo microscopes, one for dissection and one for color fundus photography.

NOTE: For transillumination to visualize pigmentary changes, use a base for dark-field microscopy.

4.2. Remove anterior segment remnants (iris and lens). To stabilize the eye during dissection, place it in the Petri dish filled with wax (Supplementary Material 1, slides 7–8). To prevent the ciliary body and attached retina from collapsing into the vitreous cavity, minimize perturbation of the ring of thick vitreous attached to the ciliary body (vitreous base).

4.3. Mark the superior pole for orientation. Place the globe anterior side down in the dish. Find the insertion tendons of the superior rectus and superior oblique muscles. Using a wooden applicator, sparingly apply a marking ink in a 10 mm line anterior to posterior direction, i.e., perpendicular to the tendinous insertion of the superior rectus muscle.

4.4. Before photography, fill the fundus with cold Sorensen's phosphate buffer.

4.5. Insert a 1 mm ruby bead into the fundus, as an internal scale bar to appear in each image[27].

4.6. Acquire color images with a single-lens reflex camera mounted to a stereo microscope fitted with a ring flash. Use trans-, epi-, and flash illumination at each of 3 standard magnifications to capture images intended to highlight specific areas (Supplementary Material 1, slide 11): 1) fundus to the equator, 2) posterior pole (vascular arcades, optic nerve head, fovea), and 3) fovea within the macula lutea (yellow spot).

5. Preparation for *ex vivo* color fundus photography

5.1. Turn the camera and monitor on. Plug in the remote shutter and release the actuator in the high-definition multimedia interface (HDMI) camera/Television (TV) monitor and display cable.

5.2. Set camera settings to manual ISO function and mirror lock-up position (locked in place, to reduce vibration). Note: refer to the manufacturer's user's manual for settings on your camera.

NOTE: Learn from the camera display the over/underexposure settings relative to the histogram and exposure readouts.

5.3. Arrange 2 light sources, each with 2 flexible light guides positioned perpendicular to each other for illumination in the 4 cardinal directions on the microscope stage (Supplementary Material 1, page 10).

5.4. Turn on epi-illumination light sources to full power.

NOTE: It is helpful but not necessary to have a black felt shroud around the stage to limit light/flash scatter for the photographer.

5.5. At the dissecting microscope, use forceps to insert the posterior pole into a 30 mL quartz crucible filled with buffer. Allow the tissue to sink to the bottom. Insert a bracing, such as a tissue sponge, between the eye and the wall of the crucible to prevent movement. Insert the 1 mm ruby bead into the posterior pole.

NOTE: The bead may fall into the optic nerve cup.

5.6. Carefully place the globe in the crucible onto the stereo microscope stage and observe the interior ocular fundus through the microscope eyepieces. Using the lowest magnification, orient the eye by identifying the tissue mark at the 12 o'clock position, the optic nerve head (ONH), and the fovea 5° below the ONH. Rotate the eye so that the fovea falls below a line through the ONH by 5°.

NOTE: If it is a right eye, the ONH is to the right of the fovea, as seen by through the oculars of the microscope. If it is a left eye, the ONH is to the left of the fovea.

5.7. Turn on the remote monitor viewing from the camera. Ensure that the microscope beam-splitter slider is set to observe through the photo port and not through the port for the oculars. Depending on the light and mirror path, be prepared to rotate the tissue 180˚ on the stage for proper orientation.

6. Image acquisition, *ex vivo* color fundus photography

6.1. With epi-illumination turned on, set the magnification so that the entire 18 mm trephine incision occupies the entire field of view. Increase magnification so that it is possible to focus on the bottom of the foveal pit. Reduce magnification to the previous setting.

6.2. Adjust ISO settings in the range of 1600–3000 so that exposure times fall in the center range of the meter on the camera.

6.3. Press the remote shutter trigger. Listen for the mirror to lock in the up position. Press the trigger again for exposure.

6.4. Observe the image on the monitor with the preset metadata showing red, green, blue (RGB), and color histogram for the correct exposure. If acceptable, proceed, if not, then delete, re-evaluate parameters, and re-image.

6.5. Turn off the gooseneck lamps for epi-illumination to highlight drusen and turn on flash at ¼ s exposure, camera shutter speed at 1/250 s, and ISO at 100–320. Set the flash speed by default or modify it at the initial set-up of the camera. Acquire an image and check the histogram for proper exposure.

6.6. Turn off the flash and turn on the trans-illumination light source. Reset ISO above 5000 and ensure the exposure time does not go below 1/30 s due to potential vibration in the photographic system. Acquire an image and check the histogram for proper exposure.

6.7. Increase magnification to view both the ONH and fovea in the field of view. Turn on epi-illumination lamps. Set ISO range to 1600–3000. Ensure that the exposure times fall in the center range of the camera.

6.8. Turn off the epi-illumination lamps, turn on the flash set to ¼ s exposure, and the preset camera shutter speed to 1/250 s and ISO set to 400–800. Acquire an image and check the histogram for proper exposure.

6.9. Turn off the flash and turn on the trans-illumination using the dark-field base. Reset ISO above 5000. Ensure that the exposure time is not slower than 1/30 s due to potential vibration in the photographic system. Acquire an image and check for a proper histogram.

6.10. Turn off the transillumination and turn on the epi-illumination lamps again.

6.11. Increase the magnification by that used in step 6.7. Refocus if needed.

6.12. Increase ISO within the range of 3000–6000 and adjust the exposure time to fall within the proper exposure range of the camera. Acquire an image.

NOTE: The ruby bead may no longer appear in the field of view. If so, capture separate images of the bead at this magnification for reference.

6.13. Turn off the epi-illumination lamps. Turn on the flash at ¼ s exposure and the camera shutter speed to 1/250 s. Set the flash speed by default or change it at the initial set-up of the camera and ISO set to 500–1000. Acquire the image. Check the histogram for proper exposure.

6.14. Turn off the flash and turn on the trans-illumination lamps. Reset ISO above 8000, to allow a faster exposure time with a more sensitive image sensor. Ensure that the exposure time does not go below 1/30 s due to potential vibration in the photographic system. Acquire an image.

6.15. Export the images from the camera into a computer. Review the images before removing the specimen from the microscope stage in case some need to be captured again.

7. Image acquisition overview for *ex vivo* OCT and scanning laser ophthalmoscopy (SLO)

7.1. For spectral domain OCT, place the globes in phosphate buffer in a custom eye holder, a chamber with a 60-diopter lens[35]. Mount the eye holder to a bracket on a clinical OCT imaging device and attach it to where a patient would rest their forehead. The OCT device automatically inserts a scale bar on each image.

7.2. At the same time, using the same device, and the eye still in the holder, image the globes with a scanning laser ophthalmoscope (SLO) in near-infrared

reflectance (NIR, used as a locator image by the indwelling software), 488 nm excitation fundus autofluorescence (FAF), and red-free (RF) reflectance.

NOTE: The 787 nm excitation FAF in this device is only occasionally suitable because a beam-splitter reduces the light transmittance to the SLO. For this reason, a second device for 787 FAF images (see next point) is used.

7.3. Separately but with the eye still in the eye holder, image the globes with 787 nm FAF for detecting RPE disturbance[36], using a separate device that displays this modality well.

8. Image acquisition protocol, *ex vivo* OCT/ SLO (see slides in Supplementary Material 2)

8.1. Indicate Superior Rectus muscle with tissue marking dye. Turn on the laser (blue arrow, Supplementary Material 2, p. 1).

8.2. Referring to page 2 of Supplementary Material 2, position the OCT head by moving the entire unit in 2 axes with respect to the base (green arrow), then raising the height (y) by rotating the joystick clockwise/ counterclockwise (cw/ ccw, blue arrows). Focus the image by rotating the knob (orange arrow), with the black lever in position R (*). Lock down the unit by securing the thumb screw (purple arrow).

8.3. Insert the eye in the holder and stabilize from the posterior aspect with spacers (Supplementary Material 1, page 13). Exert as little pressure as possible to avoid denting the sclera. Orient with the tissue mark for superior facing up.

NOTE: The approximate distance from the front of the eye holder to the OCT device is 25 mm.

8.4. Open the proprietary visualization and analysis software for the OCT device. A patient list will appear on the left column. Eye donors indexed by an internal code number are the “patients.” Refer to the user’s manual from the manufacturer.

8.5. Select the **New Patient** Icon. Complete patient data information as needed. Select **OK**. Use a logically ordered numbering system for individual eyes such as: YYYYNNNL,R_agesex. For example, 2017016R_97F.

8.6. After continuing data entry on the following window, press **OK**. Select operator and study from the drop-down menu.

NOTE: The entered information will appear in exportable meta-data.

8.7. After viewing a blank screen, touch the yellow button to start image acquisition.

8.8. Press **IR +OCT** (near infrared reflectance + OCT). Allow the laser to acquire a live SLO image of the fundus and OCT B-scan.

8.8.1. Finalize the correct anatomical position based on the ONH and fovea, using a wooden applicator to adjust the eye position in the holder. On the control panel, rotate the black round button to adjust the intensity.

8.8.2. Press the same button to average 9–100 frames (red arrows; 9 is sufficient, 100 looks creamy). If the unit is oriented correctly, the fundus should be in focus and the OCT B-scan should appear in the top third of the display (page 9, Supplementary Material 2, double red arrow).

8.8.3. On the fundus image, use the cursor to move the blue line to center the fovea (page 9, Supplementary Material 2, white arrow). Press **Acquire**.

NOTE: Other default buttons are Retina, EDI (off), and line scan.

8.9. Press **RF + OCT** for the next acquisition. Recheck the position so that the image has not moved or degraded. Press the black button for averaging. Press **Acquire**.

8.10. Switch the internal cube for autofluorescence imaging at 488 nm and 787 nm excitation wavelengths (page 10, Supplementary Material 2).

NOTE: Cube position after the switch is shown.

8.11. Select the **Autofluorescence** mode. Recheck alignment. Press **Acquire**.

8.12. For suspected cases of RPE disruption and atrophy, select **ICGA** (indocyanine green angiography) for 787 nm autofluorescence. Recheck eye position, then press **Acquire**.

NOTE: A fundus image often does not appear in this modality because the internal cube attenuates the beam.

8.13. Switch the internal cube back to **R** for IR and Red free imaging for volume acquisition.

NOTE: The cube position after the switch is shown on page 13 of Supplementary Material 2.

8.14. To acquire OCT volumes, select I**R** and the volume setting. Match all the settings on page 14 of Supplementary Material 2 by toggling the appropriate buttons on the control module (30° macula cube, 30 μm spacing, averaging to taste).

8.15. Notice that the near-infrared reflectance fundus view is covered in blue B-scan lines. Recheck OCT position in the upper third of the right window. Press **Acquire** on the **Control Module** and wait 5 min for the volume scan to complete. When imaging acquisition is completed, select **EXIT**. Images will be saved (red arrow).

NOTE: Blue lines will delimit the distances in μm, shown in the previous view. Scans will start numbering from the bottom (inferior) and proceed upward. Note the red line progression.

8.16. Allow the computer to process the acquired images, which will appear on the screen (page 16 of Supplementary Material 2).

8.17. When imaging the fellow eyes of one donor, do not change the position of the mounting bracket between the eyes. If the left eye is imaged first, results will show in the OD (right eye) column. Right-Click to select all the images, then select **exchange OS/OD**. Images will shift to the OS column.

8.18. **Select** > **Window** > **Database**. Screen defaults to panel 6 with the addition of the donor eye imaged in the right column (page 18 of Supplementary Material 2). Right-Click on the patient in the dropdown menu, choose **Batch**, and export the E2E file.

8.19. Browse to the pre-determined folder created on the desktop for file transfers. Select **OK**. The folder contains E2E files to be copied on an external hard drive and archived.

8.20. Bring the eye in its holder to the scanning laser ophthalmoscope, which is principally used for 787 nm autofluorescence. NOTE: refer to the manufacturer's user's guide for acquisition and archiving of image.

8.21. Turn on the computer and the laser.

8.22. Select **New Patient** Icon. Complete the patient data as needed.

8.23. To keep the eye datasheet the same, press **OK**. Because C-Curve stays the same, press **Continue**.

8.24. Select **Study** mode and enter the password if required. Keep the C-curve at 7.7 mm. Press **Ok**.

8.25. Select **Continue** to verify the C-curve. Select the yellow indicator to start the camera.

8.26. Select the **R** position. Align and orient the globe. Select the **IR** mode to focus and orient as above.

8.27. Orient the camera head by moving the entire unit in two axes with respect to the base (page 28, Supplementary Material 2, green arrow), then raising the height (y) of the unit (blue arrows). Focus the image by rotating the knob (orange arrow). The black lever is in position R (*). After this head is in position, lock down the unit by turning the thumb screw (purple arrow).

8.28. Notice that the screen appears as shown on page 29 of Supplementary Material 2.

8.29. Move the selector knob from **R** to **A**. Select **ICGA** (to achieve 787 nm autofluorescence) in blue, 100% intensity, 30° field of view, single phase imaging.

NOTE: Like the dye indocyanine green, melanin is excited by 787 nm wavelength light.

8.30. Notice that the screen appears as shown on page 31 of Supplementary Material 2. Press the black disc for averaging, then select **Acquire**.

8.31. Choose **Window** > **Database**. Select import E2E files from the SLO device stored on an external hard drive uploaded to the desktop.

8.32. Select open. Check marks are the default select **OK**.

8.33. Notice that the patient now has 2 tabs, one showing the images acquired from the SLO (blue arrow), and the other tab showing images acquired from the OCT device (red arrow) (see. page 34, Supplementary Materials 2).

8.34. Right-Click 786 (ICGA) image and export the picture to a file labeled SLO 786 on the desktop.

8.35. To save 786 nm autofluorescence SLO image, select patient and right-click to export images as RAW (for .vol files) to a folder on the desktop.

8.36. To export images from the OCT device for transfer to the archive computer, copy/ paste from RAWEXPORT to a folder labeled RAW.

9. Imaging review

9.1. Assemble images (color, .vol file, SLO images) in folders for each donor with subfolders for each eye, indexed consecutively by laboratory ID.

9.2. Record the tissue impressions (quality, pathology) in a database for a standardized report.

9.3. Review exported OCT volumes with an in-house ImageJ plugin.

9.3.1. Find the fovea center, recognized by the center of the foveal dip, the inward rise of the outer retinal bands, or the thinnest point. In most cases, these will coincide but not always, depending on foveal preservation, individual variability, and the presence of pathology.

9.3.2. Find a standard scan in the superior perifovea (2 mm/ 67 B-scans away in the superior direction, i.e., increasing scan numbers).

9.3.3. Save a .tif stack of the entire volume for quick reference in the future.

9.3.4. Scroll through the OCT volume in its entirety, starting from scan 1 (inferior), while recording the scan number where features are recognized.

9.3.5. Check the peripapillary area in addition to the macula.

NOTE: Peripapillary chorioretinal atrophy in older eyes includes a distinctive basal laminar deposit and neovascularization. It is a common area of pigmentary change in myopic eyes and glaucoma, in addition to aging and AMD. [37]

9.4. Inspect the color photographs and link any findings to those seen by OCT if possible.

NOTE: In general, it is easier to see most findings by OCT first. Color photographs do provide a large view of the area outside the area on the SLO, choroidal pigmentation including nevi, presence of heme and hard exudates, and black pigment in neovascular AMD. Dark pigment in the fovea may represent loose melanosomes from the anterior segment and should be washed away gently with buffer using a pipette.

9.5. Inspect the SLO images and link any findings to those seen by OCT if possible.

9.6. Save standard B-scans at the fovea and perifovea, extra B-scans with notable pathology or other features, and SLO images in a pathology report.

9.7. Categorize eyes as: Unremarkable, Questionable, Early-intermediate AMD, Atrophic AMD, Neovascular AMD, Other, Unknown, Not Gradable, Not Recorded. “Questionable” is used if it is not clear if changes are severe enough. “Not Gradable” is reserved for eyes lacking useful OCT scans, such as severely detached retinas. “Not recorded” is reserved if eyes are processed immediately upon receipt without photography.

9.8. Use these criteria for AMD: severe RPE change with either drusen or subretinal drusenoid deposits, with or without signs of neovascularization, such as fluid or fibrosis, and without evidence of other causes (updated from[10] to accommodate SDD). Note: Final diagnosis is confirmed by histologic analysis.

REPRESENTATIVE RESULTS

Table 1 shows that during 2016–2017, 184 eyes of 94 white non-diabetic donors >80 years of age were recovered. The mean death-to-preservation time was 3.9 h (range, 2.0–6.4 h). Of 184 eyes reviewed, 75 (40.2%) had certain AMD: Unremarkable (39.7%), Questionable (11.4%), Early-intermediate AMD (22.8%), Atrophic (7.6%), Neovascular (9.8%), Other (8.7%), Unknown/ Not Recorded/ Not gradable <1%. Figure 2, Figure 3, Figure 4, and Figure 5 show multiscale, multimodal *ex vivo* imaging of exceptionally well-preserved eyes from this series. Eyes were reviewed with an ophthalmologist specializing in retinal disease (JAK). While some eyes showed individual features better than others, these cases were chosen for all-around high quality.

As described[38], *ex vivo* color photography differs from *in vivo* counterparts. Retinal edema and/or detachment can reduce the visibility of posterior pigmented tissues. Observations in fresh eyes indicate that these changes occur postmortem and do not worsen markedly with prompt fixation. In addition, choroidal vessels empty after death. Due to an undulating background of pale vessels and dark interstitial tissue, the assessment of pigmentary variations in the plane of the RPE should be assisted by modalities other than color. In *ex vivo* OCT, more information is available than is seen in color photography. It also differs distinctly from *in vivo* OCT. Major differences include overall increased reflectivity of tissue, especially in the inner retina, consistent reflectivity of some bands (nerve fiber layer, inner and outer plexiform layer, RPE), lesser visibility of choroid details, especially under the edematous retina, and visibility of tissue layer detachments (see below). The outer retinal hyperreflective bands involving photoreceptors and RPE (ellipsoid zone, EZ; interdigitation

zone, IZ) are inconsistently visible *ex vivo* and are not used as landmarks in this context. The clinical consensus for spectral domain OCT uses the term RPE-Bruch's membrane band. The term RPE-basal lamina (BL)-BrM band is preferred because it accommodates the appearance of basal laminar deposits in AMD[24].

Figure 2 shows an unremarkable macula and hyporeflective large choroidal vessels, with reflective RPE-BL-BrM, between the two. A large vessel in the inner retina casts a shadow on posterior layers. The IPL and OPL are moderately reflective. In NIR SLO, both retinal and choroidal vasculatures are visible. Red-free reflectance SLO works best for features of the inner retina and vitreoretinal interfaces like arcuate fibers and papillomacular bundle of the NFL. In normal eyes, 488 nm autofluorescence SLO shows an area of overall reduced signal in the central macula due to thickened parafovea and, in some cases, absorption by yellow xanthophyll pigment, as well as hyperautofluorescence lining large retinal vessels suggestive of connective tissue sheaths. Autofluorescence at 787 nm shows a small region of increased signal in the central macula from the RPE, signal in the choroidal stroma, and hypoautofluorescent stripes corresponding to choroidal vessels.

Figure 3 shows a macula with early-intermediate AMD. Visible features include a soft druse (dome-shaped RPE elevation near the fovea), SDD (intermittent reflectivities with a dentate appearance internal to the RPE-BL-BrM band), hyperreflective foci (HRF, reflective material with the same reflectivity as in-layer RPE, located in the retina), and vitelliform change (an inward expansion of RPE organelles, both intracellular and extracellular, in conjunction with basal laminar deposit[39]). Color photography shows strong pigmentation corresponding to the vitelliform lesion, surrounded by a reduced pigmentation. Neither the drusen nor the SDD is clearly visible by color. NIR reflectance shows reflectivity in the fovea. Autofluorescence at 488 nm excitation shows a mottled signal in the fovea. SDD appears occasionally on SLO modalities, more likely if abundant, and most easily seen as a regularly spaced punctate pattern (reference[19] Figure 6). A pattern superior temporal to the fovea in Figure 3I is not SDD because it is irregular and localized to a superficial focal plane. All *en face* modalities show fine folds radiating from the fovea. In less well-preserved eyes, similar folds may be large enough to be visible at the lowest viewing magnifications.

Figure 4 shows a macula with atrophic AMD. Color fundus photography shows circular atrophic areas, central hyperpigmentation, and small hyperpigmented dots in the parafovea that correspond in OCT to HRF at the level of HFL-ONL. Also, by OCT, a low flat RPE elevation may represent basal laminar deposit, non-exudative type 1 neovascularization, or both. Atrophy in the foveal B-scan is recognizable by subsidence of the HFL-ONL, an area of hypertransmission (light shining through to choroid), vitelliform change with increased shadowing in the foveal center, and HRF that cast shadows. In this eye, NIR reflectance shows hyperreflective spots in the fovea. Autofluorescence at 787 nm excitation shows well signal corresponding to foveal hyperpigmentation and the absence of a signal in the circular atrophic areas. Red-free and 488 nm autofluorescence show inner retinal features.

Figure 5 shows a macula with macular atrophy secondary to neovascular AMD. Color fundus photography shows black pigmentation within the atrophic area. OCT shows atrophy by the sagging (subsidence) of HFL-ONL and increased hypertransmission. A foveal

B-scan shows a mound of subfoveal hyperreflective material and intraretinal cysts. Near-infrared reflectance shows reflectivity in the atrophic area due to the loss of RPE and choroidal vessels. A small, intensely reflective area in the fovea is not visible on color. Red-free reflectance shows retinal vessels and within an annular zone, choroidal vessels. Autofluorescence (488 nm) shows clearly a roughly circular atrophic border and islands of incipient atrophy. A central area devoid of the signal is surrounded by an annulus of moderate signal and visible choroidal vessels.

Figure 6 shows common artifacts in *ex vivo* OCT imaging. Edema can be prominent in the inner retina, creating bulges and folds through the fovea (Figure 6A,I). Mechanical damage can occur with traction on the vitreous or by direct contact of the retina with dissecting tools, resulting in the dislocation of material that is sometimes lost (Figure 6F,G). Detachments can occur along multiple tissue planes and may represent relative tensile forces between layers that also occur *in vivo*. Any detachment can widen further upon subsequent processing. The most common detachment is retinal, i.e., between photoreceptor outer segments and apical processes of the RPE (Figure 6B–D, F–I). The apical processes may either detach with the outer segments or remain with the RPE cell bodies, as determined by histology. Retinal detachments may be large and billowing (Figure 6B,D,I) or narrow and barely discernible (Figure 6C,F,G). Bacillary layer detachment (BALAD[40]) was first seen in the laboratory and then later found in clinical OCT. BALAD is attributed to a split through the myoid portion of photoreceptor inner segments, leaving the ellipsoid portion of the inner segment and the outer segment attached to the RPE (Figure 6A,D,I). BALAD should not be mistaken for SDD in *ex vivo* OCT. A third detachment plane is the inner limiting membrane (ILM), often with residual reflective fluid between it and the remaining retinal layers (Figure 6A,B,I). The least common detachment is between the choroid and sclera (Figure 6C). The fovea often exhibits cystoid spaces that should not be considered pathology without supporting evidence such as signs of neovascularization (Figure 6H). In single B-scans, undulations of the RPE can give the impression of drusen. The 3-D view of an OCT volume clarifies that these travel along choroidal vessels (Figure 6E,J). Undulations may be due to differential volume changes between vessels and intervening stroma after death and during fixation.

To calibrate expectations for quality and explore the limitations of *ex vivo* OCT, Figure 7 compares *in vivo* imaging, *ex vivo* imaging, and histology of three clinically documented eyes with AMD. Note that these 3 eyes were preserved differently from those in Figure 2, Figure 3, Figure 4, and Figure 5. To confirm structural OCT reflectivity sources, which are subcellular[41], eyes in Figure 7 were preserved in 2.5% glutaraldehyde and 1% glutaraldehyde to allow high-resolution epoxy resin histology and correlative electron microscopy. Glutaraldehyde adds opacity to these specimens relative to those in Figure 2, Figure 3, Figure 4, and Figure 5. The effect of shorter vs longer DtoP is apparent (Figure 7A–F, 2.1 h, vs. Figure 7G–I, 8.9 h). In the eye with longer DtoP, postmortem edema has changed the retinal contour, and the ILM is detached. Pathology of interest (outer retinal tubulation) is subtle in *ex vivo* imaging. It was found because eye-tracked *in vivo* OCT pinpointed the relevant B-scan and choroidal vessels could be matched. In the two eyes with shorter DtoP, some major pathologies (type 3 macular neovascularization) are immediately apparent (Figure 7A–C). Others are found with assistance from eye tracking (Figure 7D–F).

DISCUSSION:

Using a population-based screening approach during a 16-month period in the pre-COVID era, it was possible to procure 75 donor eyes with AMD. All were recovered with short DtoP and staged using OCT-anchored MMI. The age-criterion (>80 years) is outside the typical age range for tissue recoveries intended for transplantable corneas. Despite the advanced age, our criteria resulted eyes at all stages of AMD. Many RPE phenotypes are common to all AMD stages, and some are exclusive to neovascular AMD.[3,46] Direct comparison of *ex vivo* and *in vivo* imaging (Figure 7) confirms that short DtoP is a critical factor, along with expert handling (Figure 1), in producing *ex vivo* images of outer retina sufficient for top-level diagnostic classification with some suitable for direct imaging-histology correlations,[4,35,47] Not all pathology is visible *ex vivo.* Yet far more is visible using OCT than in color photography-based methods[10], especially those involving separating retina from RPE/choroid[27]. Further, eye tracking from clinical OCT directs attention to focal and sometime small features (Figure 7).

This preservation system involves typical eye banking procedures and tools for cornea removal, followed by immersion of an opened eye in a preservative provided in advance. In this way, eye bank personnel can recover research tissues 24/7. The latter is critical as tissues destined for immediate complex dissections[27,32] require around-the-clock staffing by either the investigators, the eye bank, or both. Other stabilizers that would enable tissue recovery at any hour followed by specialized dissection and extractions during working hours, such as PAXgene Tissue System and Hibernate-A may be helpful in the future if these are compatible with OCT imaging.

This approach yields retinas that remain largely attached to the RPE and thus capable of generating data translatable to OCT imaging. Precise localization is essential because the macula is small (<3% of retinal area). Further, deposit-driven AMD progression aligns with the topography of cones and rods, [48] and the earliest onset and most persistent visual defects occur in a specific place, i.e., rod-containing parafovea, next to the all-cone fovea. [49] For comparison to OCT, immunohistochemistry with colorimetric dyes is compatible with comprehensive microscopy (e.g., bright field) to account for all tissue elements, labeled and unlabeled[4]. Untargeted molecular assays based on sampling arrays can leverage the horizontal alignment of vertically compartmentalized photoreceptors and RPE to effectively increase resolution. Imaging mass spectrometry with ionizing laser pulses 8 μm in diameter and 10–15 μm apart can localize dozens of lipids to subcellular compartments of outer retinal cells[50]. Spatially resolved transcriptomics uses a pre-arranged set of barcoded reverse transcription primers on glass slides to which tissue sections are applied[51]. This technology is currently limited to 55 μm diameter capture and 100 μm spacing; improvements in resolution suitable for AMD research are anticipated.

This protocol has limitations. The recovery criterion omits diagnoses of diabetes (30% among Medicare recipients in Alabama)[52], due to the importance of the choroid in both diseases. This exclusion reduces the overall donor pool and lengthens the time needed to collect enough eyes for a study. For historical reasons, the 2016–2017 criteria omitted black donors, who now represent 14% of state-wide eye donors, with the inclusion of black

donors in current prospective projects. An advance directive registry for persons wishing to be eye donors is extensive but does not yet include convenient registration at local retina specialty practices that care for AMD patients, a project currently in development. During a population-based screen such as this one, eyes with conditions overlapping in phenotype with AMD will appear and must be recognized, in consultation with an evolving clinical literature and an ophthalmologist specializing in retinal disease. For example this series of eyes included nevi with drusen[53] and a line of RPE disturbance over a pachyvessel (thick vessel in inner choroid)[54]. Finally, early and intermediate AMD were combined due to the lack of an OCT-based grading system for AMD, under development by the consensus Classification of Atrophy Meeting group[55]. Nevertheless, optimization of tissue recovery and OCT-based characterization allows AMD research focused on leveraging the time element of eye-tracked OCT-anchored MMI to be planned, powered, scheduled, and budgeted for in funding applications.

Supplementary Material

Refer to Web version on PubMed Central for supplementary material.

ACKNOWLEDGMENTS:

We thank Heidelberg Engineering for instrumentation and the design of the original eye holder, Richard F. Spaide MD for introduction to OCT-based multimodal imaging, Christopher Girkin MD for facilitating access to clinical imaging devices, and David Fisher for Figure 1.The recovery of human donor eyes for research has been supported by NIH grants R01EY06019 (CAC), P30 EY003039 (Pittler), R01EY015520 (Smith), R01EY027948 (CAC, TA) R01EY030192 (Li), R01EY031209 (Stambolian), U54EY032442 (Spraggins); and IZKF Würzburg (N-304, TA), EyeSight Foundation of Alabama, International Retinal Research Foundation (CAC), the Arnold and Mabel Beckman Initiative for Macular Research (CAC), and Research to Prevent Blindness AMD Catalyst (Schey)

REFERENCES:

1. Spaide RF et al. Consensus nomenclature for reporting neovascular age-related macular degeneration data: Consensus on Neovascular Age-Related Macular Degeneration Nomenclature Study Group. Ophthalmology. 127 (5), 616–636, (2020). [PubMed: 31864668]
2. Spaide RF, Ooto S. & Curcio CA Subretinal drusenoid deposits a.k.a. pseudodrusen. Survey of Ophthalmology. 63 (6), 782–815, (2018). [PubMed: 29859199]
3. Curcio CA, Zanzottera EC, Ach T, Balaratnasingam C. & Freund KB Activated retinal pigment epithelium, an optical coherence tomography biomarker for progression in age-related macular degeneration. Investigative Ophthalmology & Visual Science. 58 (6), BIO211–BIO226, (2017). [PubMed: 28785769]
4. Cao D. et al. Hyperreflective foci, OCT progression indicators in age-related macular degeneration, include transdifferentiated retinal pigment epithelium. Investigative Ophthalmology & Visual Science. 62 (10), 34, (2021).
5. Zanzottera EC et al. Visualizing retinal pigment epithelium phenotypes in the transition to geographic atrophy in age-related macular degeneration. Retina. 36 Suppl 1 S12–S25, (2016). [PubMed: 28005660]
6. Edwards MM et al. Subretinal glial membranes in eyes with geographic atrophy. Investigative Ophthalmology & Visual Science. 58 (3), 1352–1367, (2017).
7. Zhang Z, Shen MM & Fu Y. Combination of AIBP, apoA-I, and aflibercept overcomes anti-VEGF resistance in neovascular AMD by inhibiting arteriolar choroidal neovascularization. Investigative Ophthalmology & Visual Science. 63 (12), 2, (2022).
8. Jiang M. et al. Microtubule motors transport phagosomes in the RPE, and lack of KLC1 leads to AMD-like pathogenesis. Journal of Cell Biology. 210 (4), 595–611, (2015). [PubMed: 26261180]

9. Collin GB et al. Disruption of murine Adamtsl4 results in zonular fiber detachment from the lens and in retinal pigment epithelium dedifferentiation. Human Molecular Genetics. 24 (24), 6958–6974, (2015). [PubMed: 26405179]
10. Curcio CA, Medeiros NE & Millican CL The Alabama Age-related Macular Degeneration Grading System for donor eyes. Investigative Ophthalmology and Visual Science. 39 (7), 1085–1096, (1998). [PubMed: 9620067]
11. Bastek JV, Siegel EB, Straatsma BR & Foos RY Chorioretinal juncture. Pigmentary patterns of the peripheral fundus. Ophthalmology. 89 (12), 1455–1463, (1982). [PubMed: 7162788]
12. Lewis H, Straatsma BR, Foos RY & Lightfoot DO Reticular degeneration of the pigment epithelium. Ophthalmology. 92 1485–1495, (1985). [PubMed: 4080322]
13. Lewis H, Straatsma BR & Foos RY Chorioretinal juncture. Multiple extramacular drusen. Ophthalmology. 93 (8), 1098–1112., (1986). [PubMed: 3763160]
14. Sarks JP, Sarks SH & Killingsworth MC Evolution of geographic atrophy of the retinal pigment epithelium. Eye. 2 (5), 552–577, (1988). [PubMed: 2476333]
15. Sarks JP, Sarks SH & Killingsworth MC Evolution of soft drusen in age-related macular degeneration. Eye. 8 (3), 269–283, (1994). [PubMed: 7525362]
16. Ghazi NG, Dibernardo C, Ying HS, Mori K. & Gehlbach PL Optical coherence tomography of enucleated human eye specimens with histological correlation: origin of the outer “red line”. American Journal of Ophthalmology. 141 (4), 719–726, (2006). [PubMed: 16564808]
17. Brown NH et al. Developing SDOCT to assess donor human eyes prior to tissue sectioning for research. Graefe’s Archive for Clinical and Experimental Ophthalmology. 247 (8), 1069–1080, (2009).
18. Helb HM et al. Clinical evaluation of simultaneous confocal scanning laser ophthalmoscopy imaging combined with high-resolution, spectral-domain optical coherence tomography. Acta Ophthalmologica. 88 (8), 842–849, (2010). [PubMed: 19706019]
19. Spaide RF & Curcio CA Drusen characterization with multimodal imaging. Retina. 30 (9), 1441–1454, (2010). [PubMed: 20924263]
20. Naghavi M. et al. From vulnerable plaque to vulnerable patient: a call for new definitions and risk assessment strategies: Part I. Circulation. 108 (14), 1664–1672., (2003). [PubMed: 14530185]
21. Garcia-Garcia HM, Gonzalo N, Regar E. & Serruys PW Virtual histology and optical coherence tomography: from research to a broad clinical application. Heart. 95 (16), 1362–1374, (2009). [PubMed: 19638515]
22. Strouthidis NG et al. Comparison of clinical and spectral domain optical coherence tomography optic disc margin anatomy. Investigative Ophthalmology & Visual Science. 50 (10), 4709–4718, (2009).
23. Sarks SH Ageing and degeneration in the macular region: a clinico-pathological study. British Journal of Ophthalmology. 60 (5), 324–341, (1976). [PubMed: 952802]
24. Sura AA et al. Measuring the contributions of basal laminar deposit and Bruch’s membrane in age-related macular degeneration. Investigative Ophthalmology & Visual Science. 61 (13), 19, (2020).
25. Chen L, Messinger JD, Kar D, Duncan JL & Curcio CA Biometrics, impact, and significance of basal linear deposit and subretinal drusenoid deposit in age-related macular degeneration. Investigative Ophthalmology & Visual Science. 62 (1), 33, (2021).
26. Litts KM et al. Clinicopathological correlation of outer retinal tubulation in age-related macular degeneration. JAMA Ophthalmology. 133 (5), 609–612, (2015). [PubMed: 25742505]
27. Olsen TW & Feng X. The Minnesota Grading System of eye bank eyes for age-related macular degeneration. Investigative Ophthalmology & Visual Science. 45 (12), 4484–4490, (2004).
28. Mano F, Sprehe N. & Olsen TW Association of drusen phenotype in age-related macular degeneration from human eye-bank eyes to disease stage and cause of death. Ophthalmology Retina. 5 (8), 743–749, (2021). [PubMed: 33227563]
29. Age-Related Eye Disease Study Research Group. The Age-Related Eye Disease Study system for classifying age-related macular degeneration from stereoscopic color fundus photographs: the Age-Related Eye Disease Study Report Number 6. American Journal of Ophthalmology. 132 (5), 668–681, (2001). [PubMed: 11704028]

30. Arnold JJ, Sarks SH, Killingsworth MC & Sarks JP Reticular pseudodrusen. A risk factor in age-related maculopathy. Retina. 15 (3), 183–191, (1995). [PubMed: 7569344]
31. Olsen TW, Bottini AR, Mendoza P. & Grossniklausk HE The age-related macular degeneration complex: linking epidemiology and histopathology using the Minnesota grading system (the inaugural Frederick C. Blodi Lecture). Transactions of the American Ophthalmological Society. 113 (Blodi), 1–9, (2015).
32. Owen LA et al. The Utah Protocol for postmortem eye phenotyping and molecular biochemical analysis. Investigative Ophthalmology & Visual Science. 60 (4), 1204–1212, (2019).
33. Wang JJ et al. Ten-year incidence and progression of age-related maculopathy: the Blue Mountains Eye Study. Ophthalmology. 114 (1), 92–98, (2007). [PubMed: 17198852]
34. Joachim N, Mitchell P, Burlutsky G, Kifley A. & Wang JJ The incidence and progression of age-related macular degeneration over 15 years: the Blue Mountains Eye Study. Ophthalmology. 122 (12), 2482–2489, (2015). [PubMed: 26383995]
35. Pang C, Messinger JD, Zanzottera EC, Freund KB & Curcio CA The Onion Sign in neovascular age-related macular degeneration represents cholesterol crystals. Ophthalmology. 122 (11), 2316–2326, (2015). [PubMed: 26298717]
36. Keilhauer CN & Delori FC Near-infrared autofluorescence imaging of the fundus: visualization of ocular melanin. Investigative Ophthalmology & Visual Science. 47 (8), 3556–3564, (2006).
37. Curcio CA, Saunders PL, Younger PW & Malek G. Peripapillary chorioretinal atrophy: Bruch's membrane changes and photoreceptor loss. Ophthalmology. 107 (2), 334–343, (2000). [PubMed: 10690836]
38. Curcio CA Imaging maculopathy in the post-mortem human retina. Vision Research. 45 (28), 3496–3503, (2005). [PubMed: 16171840]
39. Brinkmann M. et al. Histology and clinical lifecycle of acquired vitelliform lesion, a pathway to advanced age-related macular degeneration. American Journal of Ophthalmology. 240 99–114, (2022). [PubMed: 35192790]
40. Ramtohul P. et al. Bacillary layer detachment: multimodal imaging and histologic evidence of a novel optical coherence tomography terminology. Literature review and proposed theory. Retina. 41 (11), 2193–2207, (2021). [PubMed: 34029276]
41. Wilson JD & Foster TH Mie theory interpretations of light scattering from intact cells. Optics Letters. 30 (18), 2442–2444, (2005). [PubMed: 16196346]
42. Ghazi NG & Green WR Pathology and pathogenesis of retinal detachment. Eye. 16 (4), 411–421, (2002). [PubMed: 12101448]
43. Berlin A. et al. Correlation of optical coherence tomography angiography of type 3 macular neovascularization with corresponding histology. JAMA Ophthalmology. 140 (6), 628–633, (2022). [PubMed: 35446357]
44. Berlin A. et al. Histology of type 3 macular neovascularization and microvascular anomalies in anti-VEGF treated age-related macular degeneration. Ophthalmology Science. 2/9/23 online, (2023).
45. Schaal KB et al. Outer retinal tubulation in advanced age-related macular degeneration: optical coherence tomographic findings correspond to histology. Retina. 35 (7), 1339–1350, (2015). [PubMed: 25635579]
46. Chen L. et al. Histology and clinical imaging lifecycle of black pigment in fibrosis secondary to neovascular age-related macular degeneration Experimental Eye Research. 214 108882, (2022). [PubMed: 34890604]
47. Balaratnasingam C. et al. Histologic and optical coherence tomographic correlations in drusenoid pigment epithelium detachment in age-related macular degeneration. Ophthalmology. 124 (1), 644–656, (2017). [PubMed: 28153442]
48. Curcio CA et al. Subretinal drusenoid deposits in non-neovascular age-related macular degeneration: morphology, prevalence, topography, and biogenesis model. 33 (2), 265–276, (2013).
49. Owsley C. et al. Biologically guided optimization of test target location for rod-mediated dark adaptation in age-related macular degeneration: ALSTAR2 baseline. Ophthalmology Science. 3 (2), 100274, (2023). [PubMed: 36875335]

50. Anderson DMG et al. The molecular landscape of the human retina and supporting tissues by high resolution imaging mass spectrometry. Journal of the American Society for Mass Spectrometry. 31 (12), 2426–2436, (2020). [PubMed: 32628476]

51. Lee J, Yoo M. & Choi J. Recent advances in spatially resolved transcriptomics: challenges and opportunities. BMB Reports. 55 (3), 113–124, (2022). [PubMed: 35168703]

52. Diabetes, <https://www.alabamapublichealth.gov/healthrankings/diabetes.html> (2022).

53. Francis JH et al. Swept-source optical coherence tomography features of choroidal nevi. American Journal of Ophthalmology. 159 (1), 169–176 e161, (2015). [PubMed: 25448319]

54. Inoue M, Dansingani KK & Freund KB Progression of age-related macular degeneration overlying a large choroidal vessel. Retina Cases Brief Reports. 10 (1), 22–25, (2016).

55. Jaffe GJ et al. Imaging features associated with progression to geographic atrophy in age-related macular degeneration: CAM Report 5. Ophthalmology Retina. 5 (9), 855–867, (2021). [PubMed: 33348085]

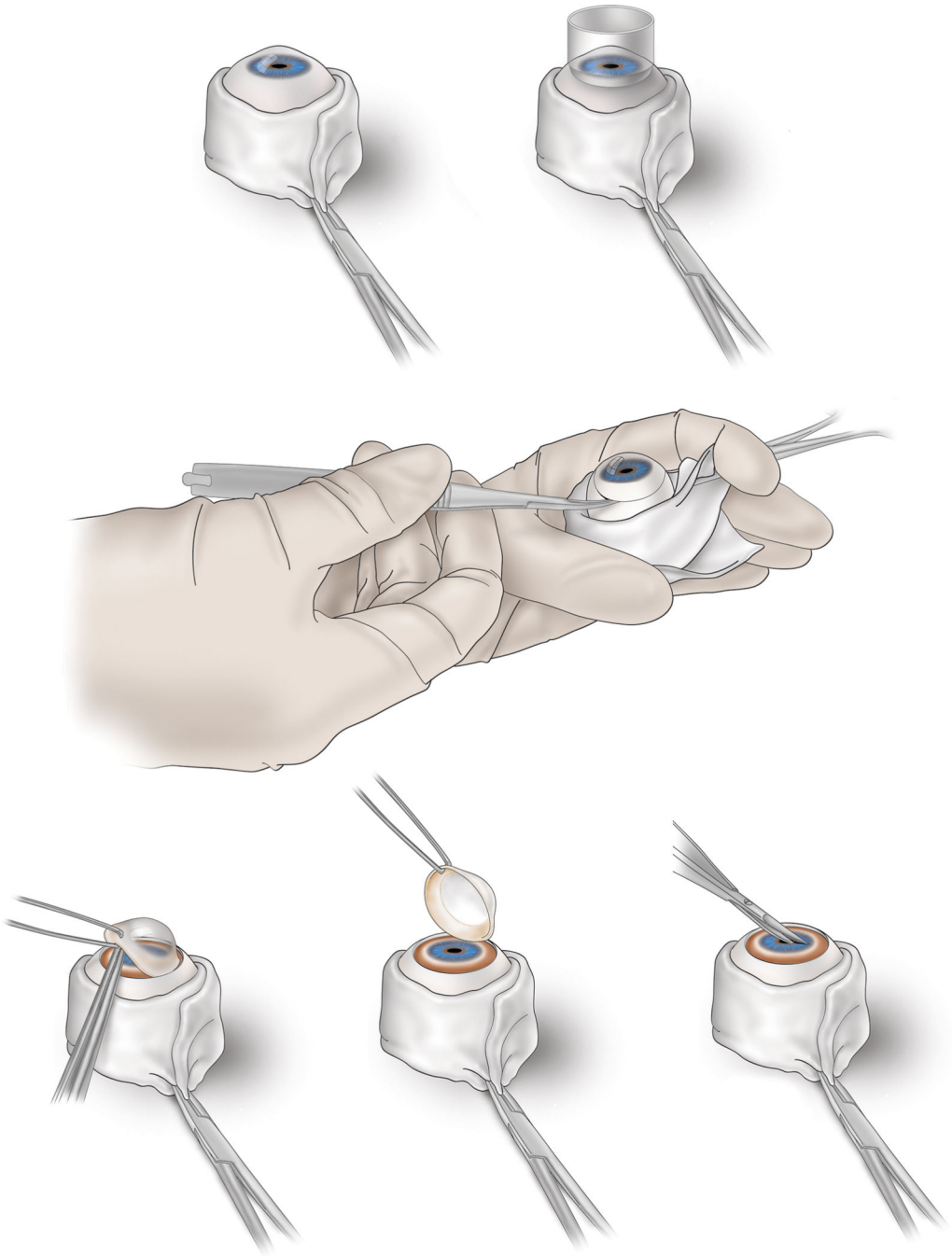

Figure 1: Corneal excision from a human donor eye for immersion fixation of the retina.
Top left, excised donor eye is held in place by a sheath of gauze stabilized by a hemostat; top right, 18 mm trephine is used to make a circular score including the cornea and a 2 mm wide rim of sclera; middle, the scored circle is finished by a cut with spring-loaded curved tipped scissors, while the globe is stabilized; bottom left, the cornea and scleral rim is lifted, exposing the iris (blue) and ciliary body (tan-brown); bottom middle, the cornea with rim is lifted off completely; bottom right, iris is snipped perpendicular to the pupillary margin to facilitate penetration of the preservative into the vitreous chamber.

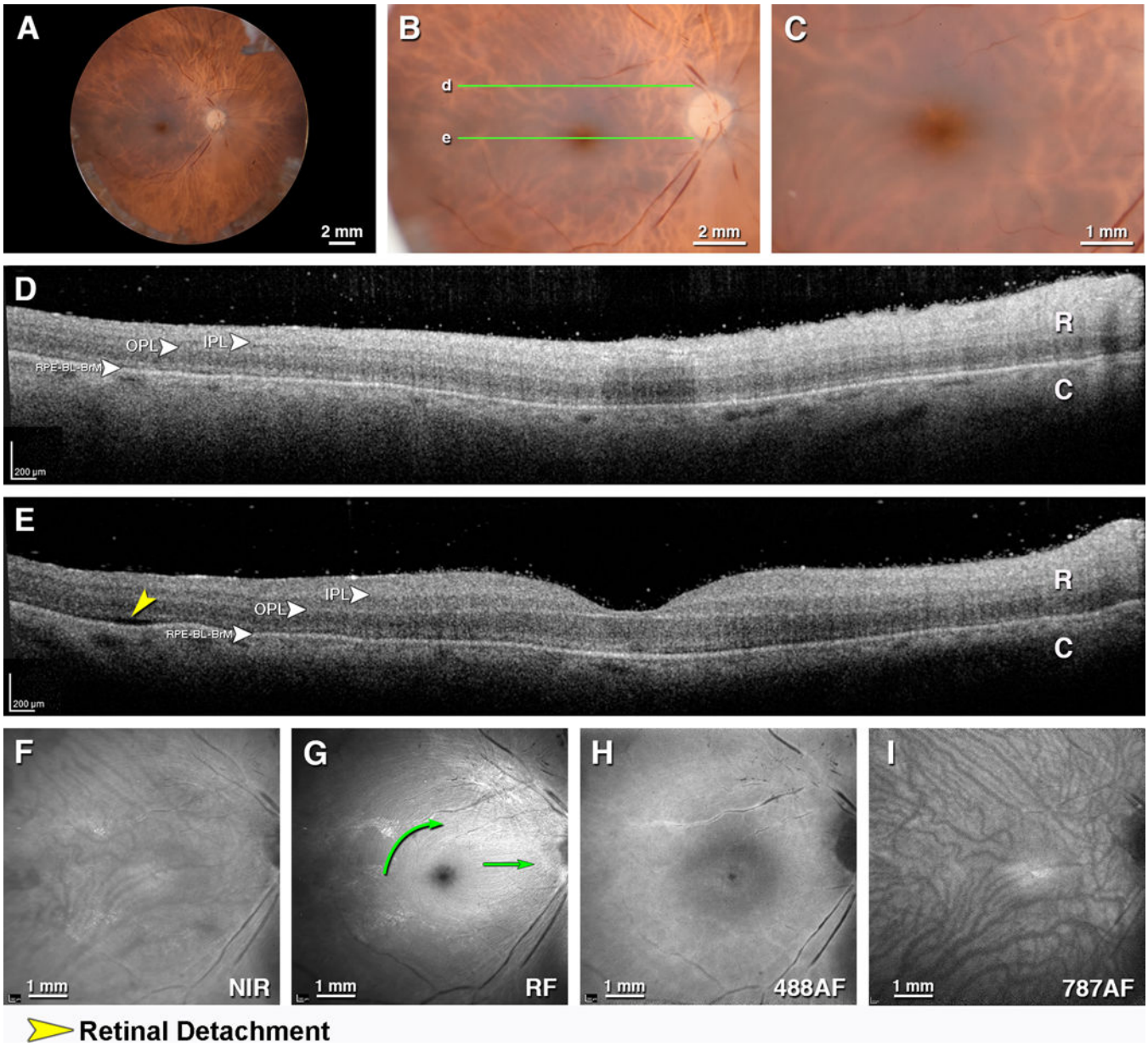

Figure 2: Multimodal *ex vivo* imaging of an unremarkable macula.

82-year-old female donor, death-to-preservation interval, 1.97 h. (**A**) Fundus of right eye viewed with anterior segment removed (epi-illumination). (**B**) Close-up of macula (epi-illumination). (**C**) Close-up view of fovea (epi-illumination). Green lines d,e indicate locations of OCT B-scans in panels **D**, and **E**. (**D,E**) OCT B-Scans through the superior perifovea (d) and fovea (e). Retina (R), choroid (C) with hyporeflective large vessels, and intervening hyperreflective RPE-BL-BrM are visible. In this exceptionally well-preserved eye, the moderately reflective IPL and OPL are also visible. (**D**) A large vessel in inner retina casts a shadow on posterior layers. (**E**) Separation between retina and RPE in E (yellow arrowhead) is artifactual. (**F**) Near infrared reflectance shows detail of both retinal and choroidal vasculatures. (**G**) Red free reflectance shows arcuate fibers (left green curved

arrow) and papillomacular bundle (green arrow) of the nerve fiber layer. (**H**) 488 nm wavelength autofluorescence shows an area of overall reduced signal in the central macula due to thickened edematous parafovea, as well as rings and a point of low signal in the foveal center and hyperautofluorescence lining large retinal vessels suggestive of connective tissue sheaths. (**I**) 787 nm autofluorescence showing a small region of increased signal in central macula from the RPE, signal in the choroidal stroma, and hypoautofluorescent stripes corresponding to choroidal vessels.

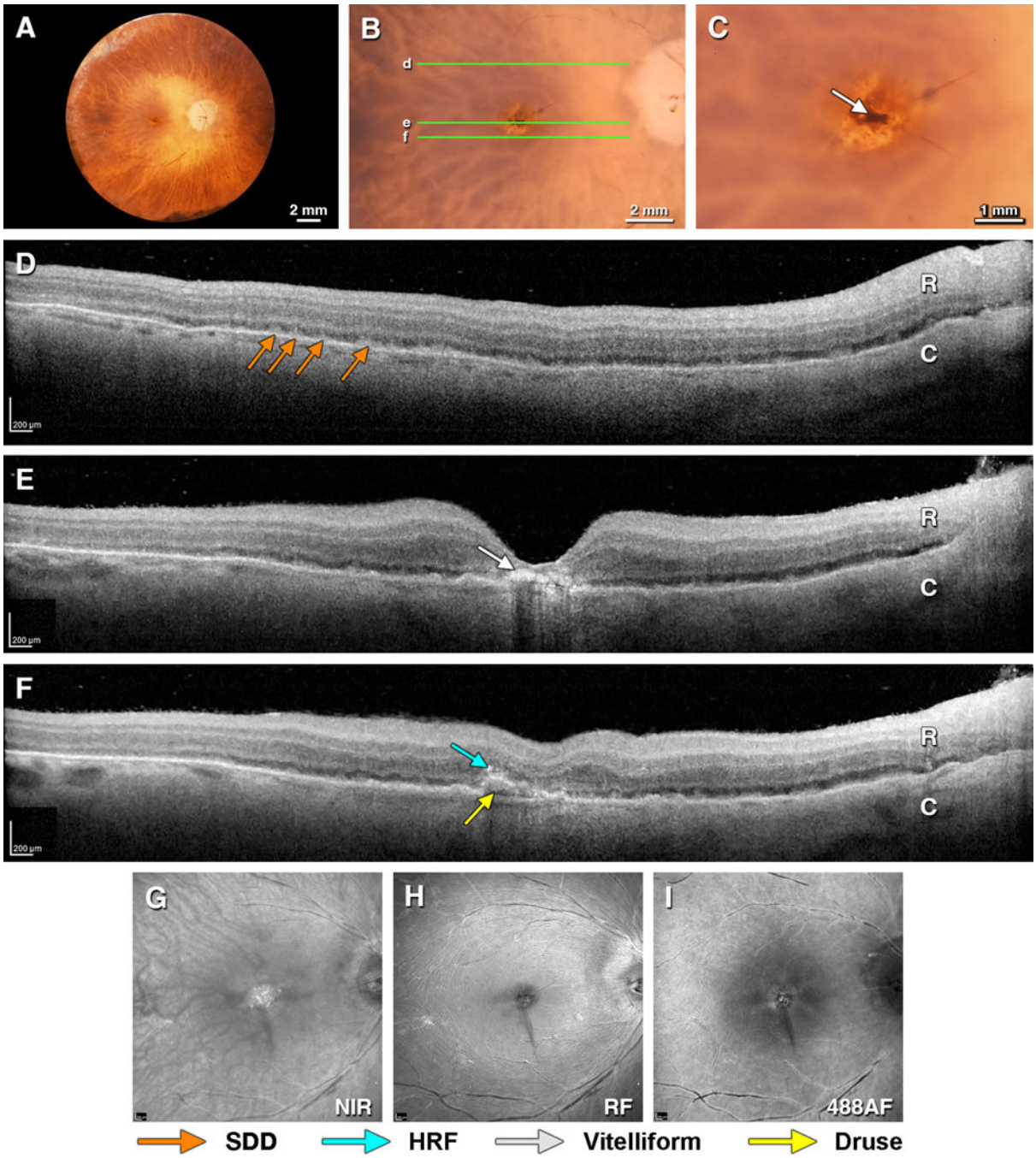

Figure 3. Multimodal ex vivo imaging of donor eye with early intermediate AMD.

97-year-old-female donor, death-to-preservation interval, 3.1 h. (**A**) Fundus of right eye viewed with anterior segment removed (epi-illumination). (**B**) Close-up of macula (epi-illumination). Green lines d, e, f indicate locations of OCT B-scans in panels D,E, and F. (**C**) Close-up view of fovea showing hyperpigmentation (arrow, flash illumination). (**D**) SDD in superior perifovea (orange arrows) is seen on OCT. (**E**) Vitelliform change of RPE under the fovea (white arrows). (**F**) Inferior to fovea is a soft druse with hyporeflective line at the base (yellow arrow) and a hyperreflective focus, above (light blue arrow). (**G–I)**

Scanning laser ophthalmoscope images show very fine stellate folds in fovea (also seen in C). (**G**) Near infrared reflectance shows reflectivity material in the fovea corresponding in part to vitelliform material. (**H**) Red-free reflectance shows the retinal surface. (**I**) 488 nm wavelength autofluorescence shows an area of overall reduced signal in the central macula due to slightly thickened parafovea. SDD are not clearly visible.

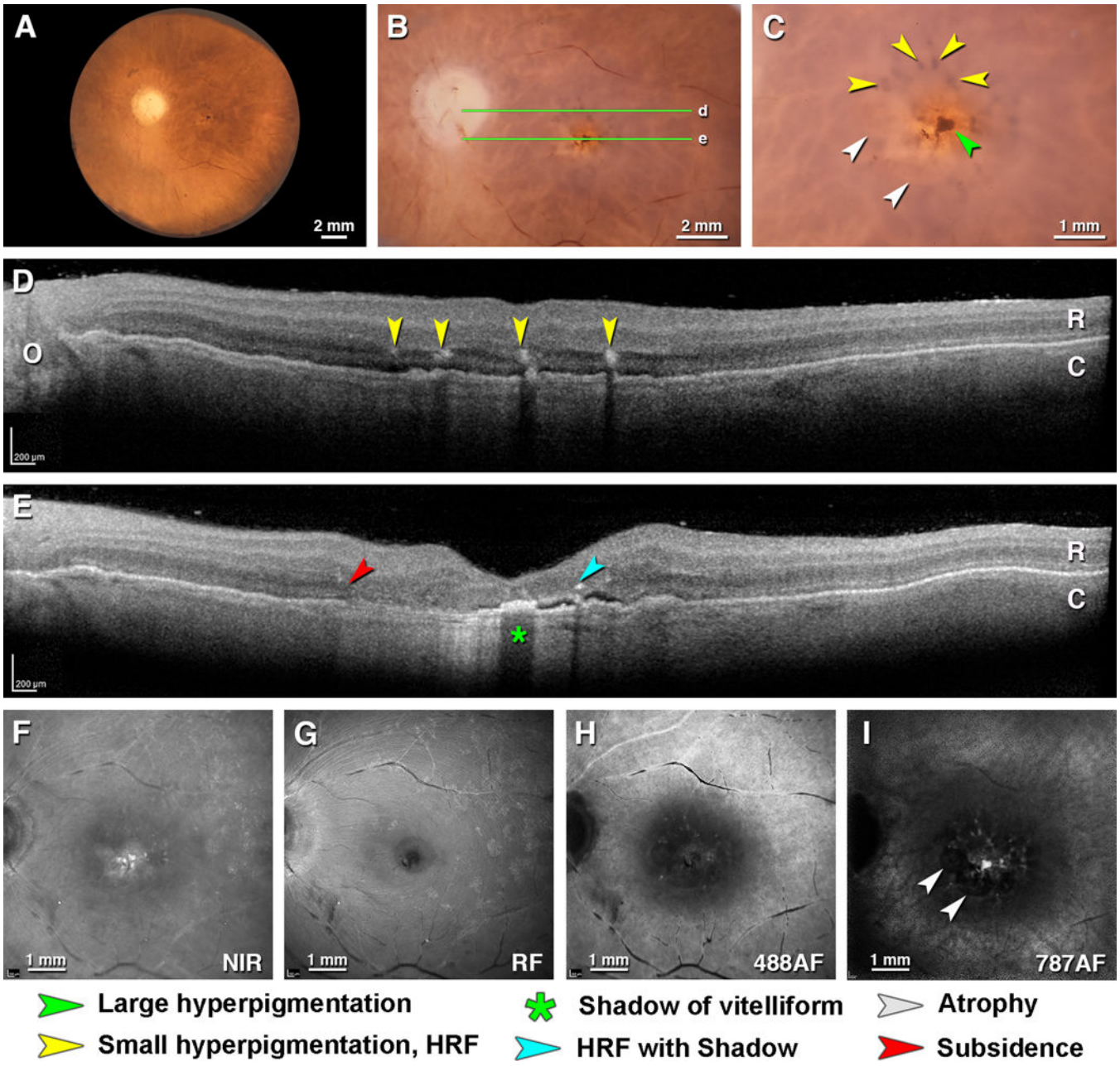

Figure 4: Multimodal ex vivo imaging of complete RPE and retinal atrophy in age-related macular degeneration.

97-year-old female, death-to-preservation interval, 2.33 hours. (**A**) Fundus of left eye viewed (trans-illumination). (**B**) Close-up of macula (epi-illumination). Green lines d,e indicate locations of OCT B-scans in panels D, and E. (**C**) Close-up of fovea (epi-illumination) showing central hyperpigmentation (green arrowhead) and small hyperpigmented dots (yellow arrowheads). The central dot is intense brown because the overlying retina is very thin. The dots appear desaturated because the overlying retina is thick. Circular atrophic areas are indicated (white arrowheads). (**D, E**) OCT B-Scans through the perifovea (d) and fovea (e). Retina (R) and thin choroid (C) are visible. (**D**) Hyperreflective foci (yellow

arrowheads) at level of HFL-ONL correspond to hyperpigmented dots in C. A low flat RPE elevation under them may represent basal laminar deposit, non-exudative type 1 neovascularization, or both. (**E**) B-scan through the fovea shows atrophy recognizable by subsidence of the HFL-ONL (red arrowhead), an area of hypertransmission, vitelliform change with increased shadowing in the foveal center (green asterisk), and hyperreflective foci (teal arrowhead) with shadowing. The hyporeflective space between retina and RPE band may represent subretinal fluid. (**F**) Near infrared reflectance shows hyperreflective spots in the fovea. (**G**) Red free image shows arcuate fibers of the NFL and reflective blooms on the retinal surface. (**H**) 488 nm autofluorescence focused on retina shows signal associated with retinal vessels, not signal associated with RPE, and faint autofluorescent spots in central macular area. (**I**) 787 nm autofluorescence shows signal corresponding to the pigmentation in C. Circular atrophic areas are apparent.

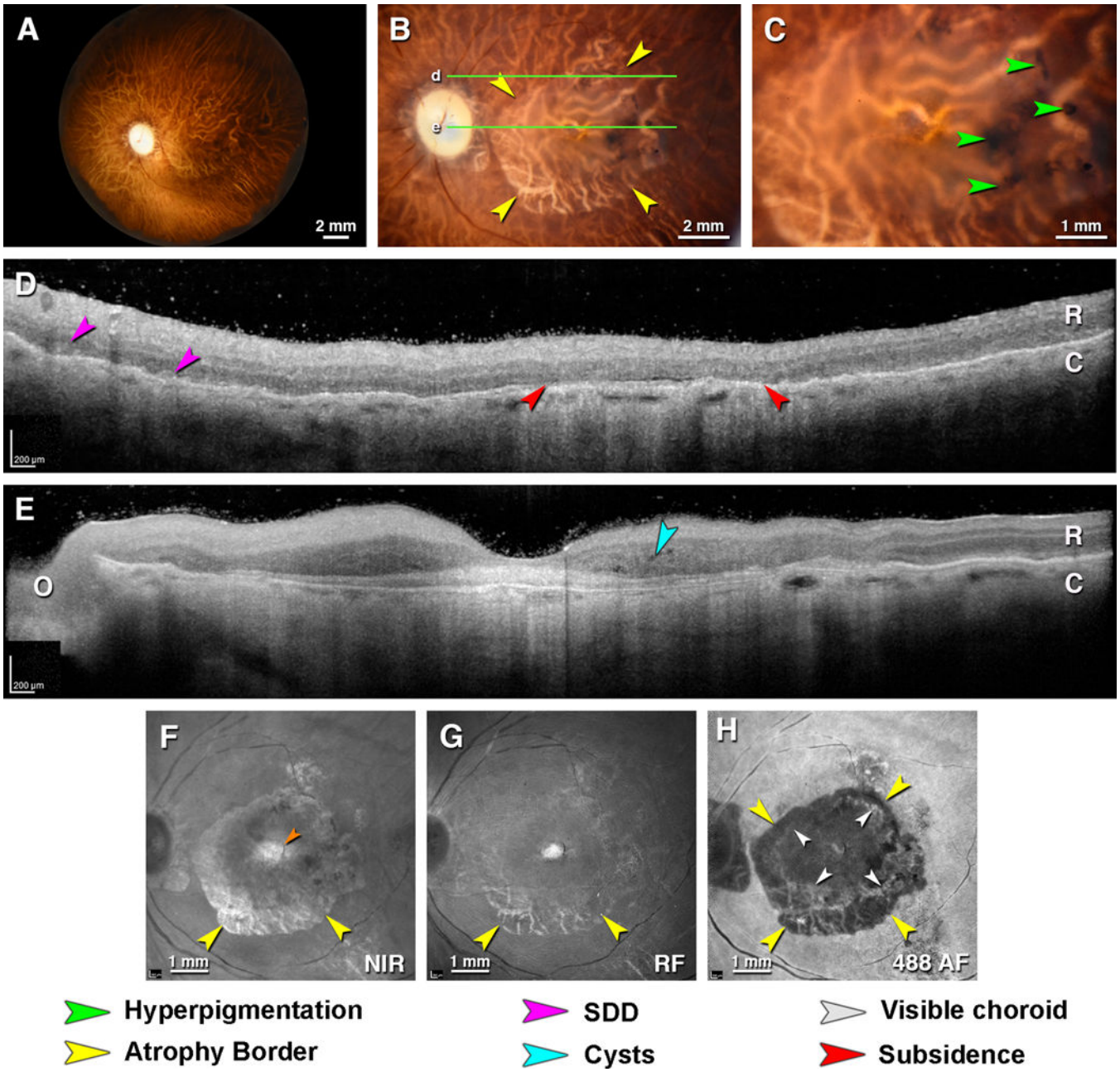

Figure 5: Multimodal ex vivo imaging of type 1 neovascularization and macular atrophy in age-related macular degeneration.

86-year-old female donor, death-to-preservation interval, 3.5 h. (**A**) Fundus of left eye viewed with anterior segment removed (trans-illumination). (**B**) Close-up of macula detailing atrophy borders (yellow arrowheads). Green lines d,e indicate locations of OCT B-scans in panels D, and E. (**C**) Close-up of fovea shows black pigmentation (green arrowheads) within the atrophic area. (**D, E**) OCT B-Scans through the perifovea (d) and fovea (e). Retina (R) and thin choroid (C) are visible. In this exceptionally well-preserved eye, the moderately reflective IPL and OPL are also visible. (**D**) Perifoveal B-scan grazes the superior edge of the atrophic area. Atrophy is evidenced by the

sagging of HFL-ONL and increased hypertransmission (red arrowheads). Possible subretinal drusenoid deposits are indicated (fuchsia arrowheads). (**E**) Foveal B-scan shows a mound of subfoveal hyperreflective material and intraretinal cysts (asterisk). O, optic nerve head. (**F**) Near infrared reflectance shows a reflective area of atrophy and choroidal vessels (teal arrowheads), including small intense area in central macula (orange arrowhead) not visible by color imaging. (**G**) Red free reflectance shows retinal vessels and within an annular zone, choroidal vessels. (**H**) 488 nm autofluorescence depicting a roughly circular atrophic border (yellow arrowheads) and islands of incipient atrophy. a central area devoid of autofluorescence is surrounded by an annulus of moderate autofluorescence and visible choroidal vessels (white arrowheads). 787 nm autofluorescence was not possible in this eye.

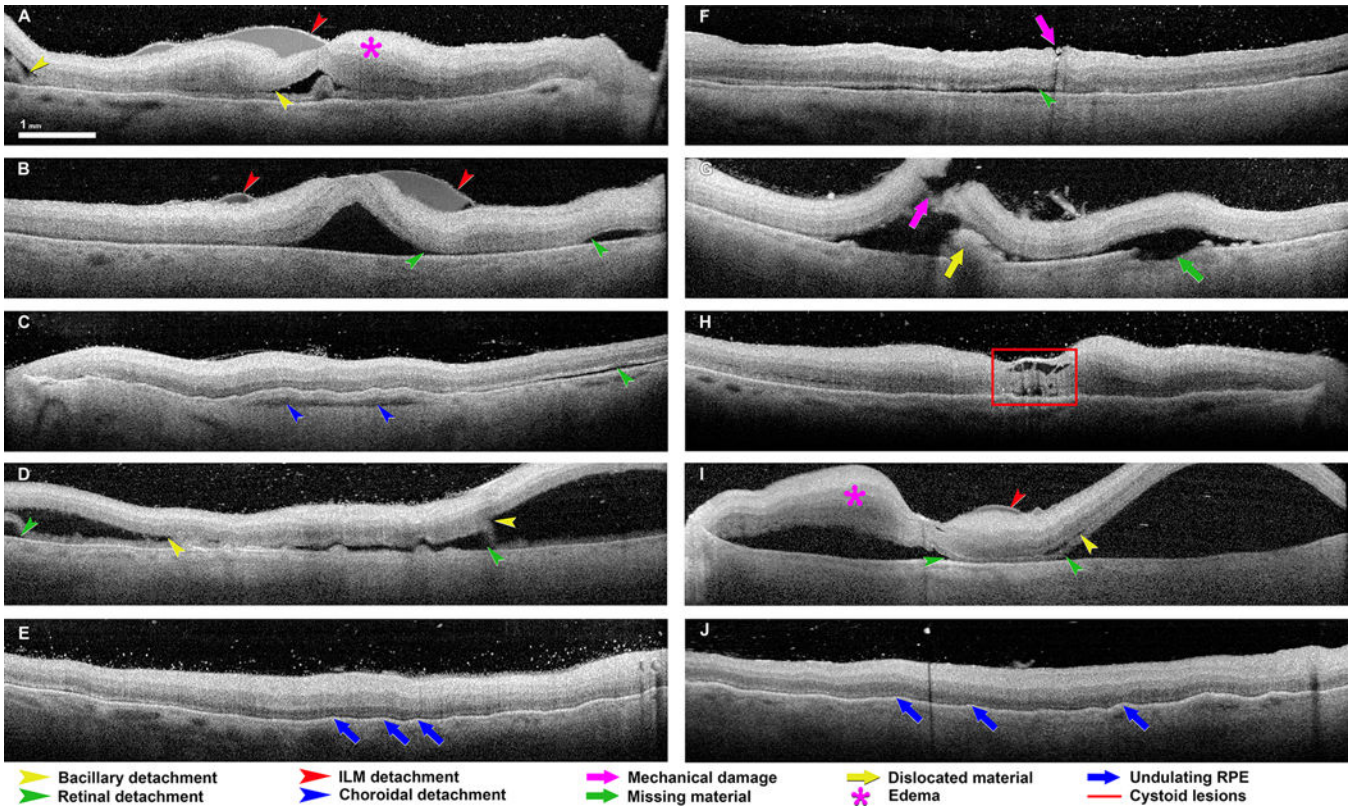

Figure 6: Common artifacts seen in ex vivo OCT imaging of donor eyes.

From the 2016–2017 series of eyes. Most retinas are hyperreflective relative to retinas imaged *in vivo,* with the inner retinal layers more reflective than outer retinal layers. Bacillary detachment (yellow arrowhead in panels **A, D, G,** and **I**) is defined as a split at the level of the photoreceptor inner segment myoid creating a distinctive intraretinal cavity[40]. Retinal detachment (green arrowhead in panels **B, C, D, F,** and **G, I**) describes a separation of the entire neurosensory retina from the underlying RPE[42]. Detachments of the internal limiting membrane (ILM) separate the ILM and nerve fiber layer (red arrowhead in panels **A, B,** and **I**). A choroidal detachment (blue arrowhead in panel **C**) is a separation within the choroid or between the choroid and sclera. Mechanical damage (purple arrow in panels **F,** and **G**) can appear at any level and with any dimensions, as applies to missing material (green arrow in panel **G**) and dislocated material (yellow arrow in panel **G**). Retinal edema (purple star in panels **A,** and **I**) appears as a thickening of retinal tissue with poorly defined boundaries between the separate retinal layers. Undulating RPE (blue arrow in panels **E,** and **J**) appears as an uneven, wavy RPE layer. Cystoid lesions (red square in panel **H**) correlate to hyporeflective chamber like alterations within the retinal tissue, commonly in the fovea.

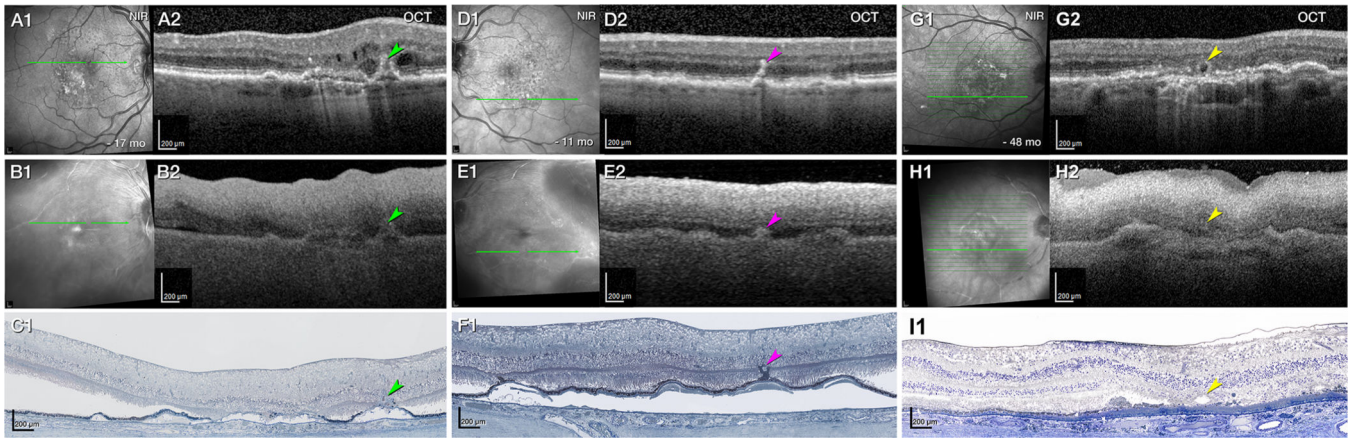

Figure 7: *Ex vivo* visibility of pathology seen *in vivo* depends on preservation quality.

(A–I) Panels **A, B,** and **C,** panels **D, E,** and **F,** and panels **G, H,** and **I** represent three clinically documented eyes of two donors, each seen by eye-tracked *in vivo* (**A1–A2, D1–D2, G1–G2**) and *ex vivo* (**B1–B2, E1–E2, H1–H2**) imaging, followed by histology (**C, F, I**). Green lines on near-infrared reflectance (NIR, **A1, B1, D1, E1, G1, H1**) represent the levels of optical coherence tomography (OCT) B-scans and panoramic histology. Panels **A, B,** and **C,** and panels **D, E,** and **F,** are right and left eye, respectively, of one female donor in her 90's. Panels **G, H,** and **I** show the right eye of a second female donor, also in her 90's. (**A–C**) Well-preserved ocular tissue (DtoP, 2.1 h) enables good visibility of major pathology. (**A**) A hyperreflective intraretinal macular neovascularization (type 3 MNV, green arrowhead) is surrounded by intraretinal fluid, 17 months before death (**A2**). The RPE/Bruch's membrane complex is split by hyporeflective material and appears as a "double layer" sign (**A2**). To the left is another double layer sign with barcode hypertransmission into the choroid (orange arrowhead). On *ex vivo* OCT (**B2**) the type 3 MNV and barcode hypertransmission are clearly visible and delineated. Retina is artifactually detached, white arrowhead. Panoramic histology shows a vertically oriented type 3 MNV lesion (green arrowhead, **C1**). See [43,44] for details of original case. (**D–F**) Well-preserved ocular tissue (DtoP 2.1 h) can result in transparency that is reduced yet still sufficient for detecting major pathology. OCT (**D2**) shows a stack of intraretinal hyperreflective foci (HRF, fuchsia arrowhead) in an eye followed for exudative type 3 MNV. No intraretinal cysts are visible, 11 months before death. On *ex vivo* OCT (**E2**) the stack of HRF is compressed vertically (fuchsia arrowhead) but clearly delineated. On panoramic histology (**F1**), a retinal pigment epithelium tower (fuchsia arrowhead) rises upward from a soft druse. (**G–I**) Less well-preserved ocular tissue (DtoP, 8.9 h) results in reduced visibility of major pathology. OCT indicates an outer retinal tubulation (ORT, yellow arrowhead), 48 months before death (**G2**). On ex vivo OCT, the ORT appears as a subtle disturbance and would have been difficult to discern without prior knowledge (**H2**). The inner limiting membrane is artifactually detached (white arrowhead). Edema has distorted the retinal contour. Histological analysis shows the ORT lumen delimited by the external limiting membrane and photoreceptors protruding into it (**I1**). See[26,45] for details of original case.

Table 1.

Donor eye recovery 2016–2017

	Numbers			Percentages		
Diagnostic category	**Right Eyes**	**Left Eyes**	**Total**	**Right Eyes**	**Left Eyes**	**Total**
Unremarkable	39	34	73	41.50%	37.80%	39.70%
Questionable AMD	10	11	21	10.60%	12.20%	11.40%
Early AMD	20	22	42	21.30%	24.40%	22.80%
Atrophic AMD	6	8	14	6.40%	8.90%	7.60%
Neovascular AMD	11	7	18	11.70%	7.80%	9.80%
Other	7	8	15	7.40%	8.90%	8.20%
Unknown	0	0	0	0.00%	0.00%	0.00%
Not recorded	1	0	1	1.10%	0.00%	0.50%
Total	**94**	**90**	**184**	**100.00%**	**100.00%**	**100.00%**
Certain AMD	**37**	**37**	**75**	**39.40%**	**41.10%**	**40.20%**
Possible AMD	**47**	**48**	**95**	**50.00%**	**53.30%**	**51.60%**

Eyes were accessioned during the period 6/17/16 – 9/14/17. Criteria: ≥ 80 years, white, non-diabetic, ≤6 h death-to-preservation. Target: 184 eyes (180 eyes of 90 donors, preserved; 4 eyes of 4 donors, preserved) Death-to-preservation time (mean, maximum, minimum): 3.9 h, 6.4 h, 2.0 h